Inferring Cloud Feedbacks from
ARM Continuous Forcing, ISCCP, and ARSCL Data

A. D. Del Genio
National Aeronautics and Space Administration
Goddard Institute for Space Studies
New York, New York

A. B. Wolf and M.-S. Yao
SGT Inc., Institute for Space Studies
New York, New York

Introduction

Single Column Model (SCM) versions of parent general circulation models (GCMs), accompanied by cloud-resolving models (CRMs) that crudely resolve cloud-scale dynamics, have increasingly been used to simulate limited time periods of observations, driven not so much by specific science questions but by the availability of field experiment data or enhanced soundings during Intensive Observation Periods (IOPs). These exercises have provided limited insights about either climate or cloud parameterization, because it usually cannot be determined whether model-data discrepancies are due to inaccurate large-scale advective forcing or inaccurate model physics, and in any case the errors revealed may not be climatically representative or indicative of a shortcoming in the model's cloud feedback prediction

To the extent that climate change manifests itself as a change in the frequency of occurrence of current atmospheric states, as opposed to the onset of previously unrealized states, it might be possible to learn something about cloud responses to climate forcing if examples of configurations characteristic of the future climate can be identified in current climate records. In climate general-circulation models the direct radiative heating/cooling perturbation due to the greenhouse gas increase itself is small except at the surface and tropopause. Instead, strong positive feedbacks associated with changes in water vapor and snow-sea ice are primarily responsible for the altered thermodynamic structure of the warmer climate. In many situations clouds are a tracer of the general circulation, i.e., they are a response to the advection of heat and moisture. Cloud feedbacks can therefore be viewed as the response to anomalous advective tendencies caused by climate changes in the circulation and the temperature and moisture gradients along which they advect. Having defined those tendencies in general-circulation model climate change simulations and found current climate examples of similar tendencies, it should be possible to use simultaneous cloud observations to define the cloud type changes that are consistent with the altered dynamical state.

A major drawback to such an approach is the general unavailability of accurate instantaneous information about the general circulation in most climate regimes. Reanalysis products are most tightly constrained by observations in northern midlatitudes, and even there, the dynamical response is often muted in the presence of unresolved diabatic heating. IOPs with a large-scale array of enhanced

soundings provide more accurate dynamical tendencies but also not without errors and with at best only an example or two of the desired dynamical conditions given their short duration. A recent promising alternative is the "continuous forcing" dataset derived by Xie et al. (2004) at the Atmospheric Radiation Measurement (ARM) Program's Southern Great Plains (SGP) site. The continuous forcing product modifies the mesoscale analysis from the Rapid Update Cycle – 2 system using a constrained variational analysis approach. Xie et al. show that the continuous forcing product is often of comparable quality to that from IOPs, but with the advantage of being available for climatically significant periods of time (two years have been processed thus far).

This extended abstract describes a first attempt to implement the philosophy described above to observationally constrain regional cloud feedbacks and to evaluate the ability of the Goddard Institute for Space Studies (GISS) SCM to simulate them. This work has also been submitted for publication to an ARM special issue of *Journal of Geophysical Research.*

Approach

Weather at the SGP site is controlled by baroclinic wave activity and frontal passages. Superimposed diurnal variations and deep convection occur more frequently in summer, while winter variability is more purely synoptic in nature. It is at this time of year that we expect clouds to be most nearly a response to synoptic forcing rather than a determinant of the forcing. Thus, we select 5 cold season months of continuous forcing (January-March, November-December) in the 2 available years (1999-2000) to drive the GISS SCM. The SCM physics is similar to that in the SI2000 version of the GISS general-circulation model, but includes several recent updates of cloud and convection physics, as described by Del Genio et al. (2004). We run the SCM with 35 layers matched to the resolution of the hourly continuous forcing advective tendencies of temperature and specific humidity. The SCM is re-initialized every 24 hr with the observed thermodynamic profiles to avoid obscuration of the cloud response by climate drift.

We use two complementary datasets to characterize the cloud structure at the SGP during these 10 months. The International Satellite Cloud Climatology Project (ISCCP) D1 data (Rossow and Schiffer 1999) provide joint distributions of cloud top pressure and total column optical thickness at ~5 km resolution sampled to ~30 km every 3 hr during daytime for areas comparable to the size of a general-circulation model gridbox. The top pressure corresponds to the highest cloud; multilayer cloud situations cannot be distinguished. The retrieval technique, using visible and window infrared radiances, does not detect very optically thin clouds and sometimes incorrectly locates the top of clouds it does detect, usually due to inadequate information about the instantaneous humidity and temperature structure.

The active remote sensing of cloud layers (ARSCLs) product (Clothiaux et al.2000) combines millimeter cloud radar and micropulse lidar data to derive a best estimate of the altitudes of all cloud bases and tops in a narrow field of view looking upward at the SGP central facility. The results are considered accurate except for occasional underestimates of cloud top in deep heavily precipitating cloud systems. However, they are representative of an area much smaller than a general-circulation model gridbox. Comparison to the SCM is simplified by the fact that we aggregate statistics over many events rather than making instantaneous comparisons. ARSCL cloud profiles are compiled at 10-s

intervals; we aggregate them over each hour and create joint distributions of cloud top height and total cloud physical thickness (highest top minus lowest base) as a geometric cloud property counterpart to the ISCCP radiative property distributions.

To compare the satellite observations to the model, hourly SCM cloud fields are diagnosed using the ISCCP simulator (Klein and Jakob 1999, Webb et al. 2001). We also take 100 subgrid columns of overlapping cloud produced by the ISCCP simulator as input to create a crude "ARSCL simulator." For each hour we randomly select one of the columns plus the three adjacent columns as a representative sample of the atmospheric volume observed by the active sensors over the hour, given typical cold season mid-tropospheric wind speeds at the SGP.

From this 10-month record of cold season cloudiness variability, we select time periods that are most relevant for understanding cloud feedbacks in a climate change. To do so, we use equilibrium $2xCO_2$ and $1xCO_2$ simulations of the GISS general-circulation model. Each of the equilibrated runs is sampled hourly for 10 years at the SGP and three nearby gridboxes. At each gridbox and timestep advective tendencies of temperature and humidity and ISCCP/ARSCL simulator cloud histograms are saved. The differences between these quantities for the warmer minus control climate, averaged over the ten years, define the climate change advective forcing anomalies and the associated cloud response that determines the regional cloud feedback. We separate the anomalies by the sign of the 500 mb vertical velocity ω, since upwelling and downwelling segments of baroclinic waves have characteristically different cloud structures and should not be expected to respond in the same way to climate forcing.

We then correlate the vertical profiles of warm-control advective tendency differences with the instantaneous advective tendency anomalies in the continuous forcing data (relative to the 10-month mean tendency profiles) for $\omega < 0$ and $\omega > 0$. Those timesteps whose temperature and moisture tendency anomaly profiles are correlated with those from the climate change simulation at the 95% confidence level or higher (correlation coefficient $r > 0.417$) are selected as being representative of the climate change signal. The observed ISCCP/ARSCL histograms averaged over those times are interpreted as an indicator of what the atmosphere's actual regional response to such climate forcings would look like. Comparison of these observed cloud anomalies to those simulated by the SCM at the same times tests the fidelity of the model cloud feedbacks. Finally, comparison of the SCM-simulated anomalies to the $2xCO_2$ cloud changes tells us how relevant the observed current climate variability is to the actual cloud feedbacks.

Several caveats must be stated. (1) A general-circulation model climate change simulation is only available for an earlier version of the model physics (cf. Yao and Del Genio 2002) at much coarser vertical resolution than for the SCM and continuous forcing (9 layers as opposed to 35). Several effects of the resolution difference in particular will be apparent in what follows. (2) Climate change is actually a shift in the entire probability density function (PDF) of advective tendencies rather than just a change in the mean values for upwelling and downwelling situations. Ideally one would treat the changes separately for weak, intermediate, and strong vertical velocities of both signs. However, the 2-year length of the currently available continuous forcing dataset is not sufficient to accumulate sufficient statistics in a large number of ω bins. (3) We have ignored the contributions of surface turbulent fluxes and the $2xCO_2$ radiative heating anomaly itself to the tendencies. In midlatitude winter, surface fluxes should either be small or correlated with specific dynamical anomalies (e.g., cold air outbreaks), so the

former should not be an issue. The radiative heating anomaly is an order of magnitude smaller than the peak dynamical heating anomaly, but it is non-negligible relative to the advective anomaly near the surface. (4) The best matches to the climate change advective tendencies in the continuous forcing are not perfect, and this may account for some of the differences we observe in the sections that follow.

Mean Forcings and Cloud Distributions

Figure 1 shows the 10-month mean continuous forcing temperature and moisture advective tendency profiles for $\omega < 0$ and $\omega > 0$. Temperature tendencies are characterized by adiabatic cooling, peaking near 500 mb, in upwelling regimes but changing sign to adiabatic warming near 300 mb, presumably a signature of sloping frontal surfaces. In downwelling regimes the opposite is true although the forcing has a broader and lower altitude peak and slightly smaller peak magnitudes. Moisture tendencies are defined by moistening/drying in upwelling/downwelling situations, respectively, again with weaker magnitude and a lower altitude peak in downwelling cases (900 vs. 750 mb).

Also shown for comparison in Figure 1 are the control simulation advective tendency profiles from the free-standing general-circulation model for the SGP region. General-circulation model advective forcings have the same general pattern as those in the continuous forcing but are noticeably weaker and shallower in depth in upwelling regions. This may be a reflection of the inability of climate general-circulation models to resolve mesoscale secondary circulations along fronts.

Figure 2 shows mean observed and simulated cloud property histograms for the $\omega < 0$ regime. ISCCP retrievals (upper left) suggest 4 dominant cloud types in these situations: low optically thick clouds (suggestive of stratus) with tops near ~600-700 mb, high optically thick clouds (nimbostratus and perhaps some cumulonimbus) with tops near ~300-400 mb, optically thin cirrus at similar top pressures, and a class of very optically thin clouds near the tropopause. The latter cloud category is known to include some artifacts associated with situations in which ISCCP cannot uniquely identify the actual cloud top.

ARSCL retrievals (Figure 2, lower left) indicate some similarities and some differences in this overall picture, keeping in mind the different space and time scales associated with the passive and active sensors. ARSCL detects physically thin and thick high clouds with tops at ~9-11 km, consistent with two of the ISCCP high cloud types. However ARSCL detects no tropopause thin cirrus, reinforcing the impression that this feature is an artifact of ISCCP limitations in optically thin cloud situations. ARSCL detects a low physically thin cloud category but with tops at ~1-2 km, well below the ~600-700 mb ISCCP cloud top inference. The SCM (Figure 2, upper and lower middle) does a fairly good job in simulating the observed cloud types. It captures both high cloud types at the correct top pressures, though its optically thin clouds are too thin and its optically thick clouds too thick. It also simulates the low thin cloud category at almost the same altitude as inferred from the ARSCL data. The most notable real discrepancy between the data and the SCM is that the latter tends to make far too many thick high clouds. We will return to this problem in the next section.

The general-circulation model (Figure 2, upper and lower right) differs from the SCM and the observations in its inability to make thin cirrus. This may be a consequence of its coarse resolution in
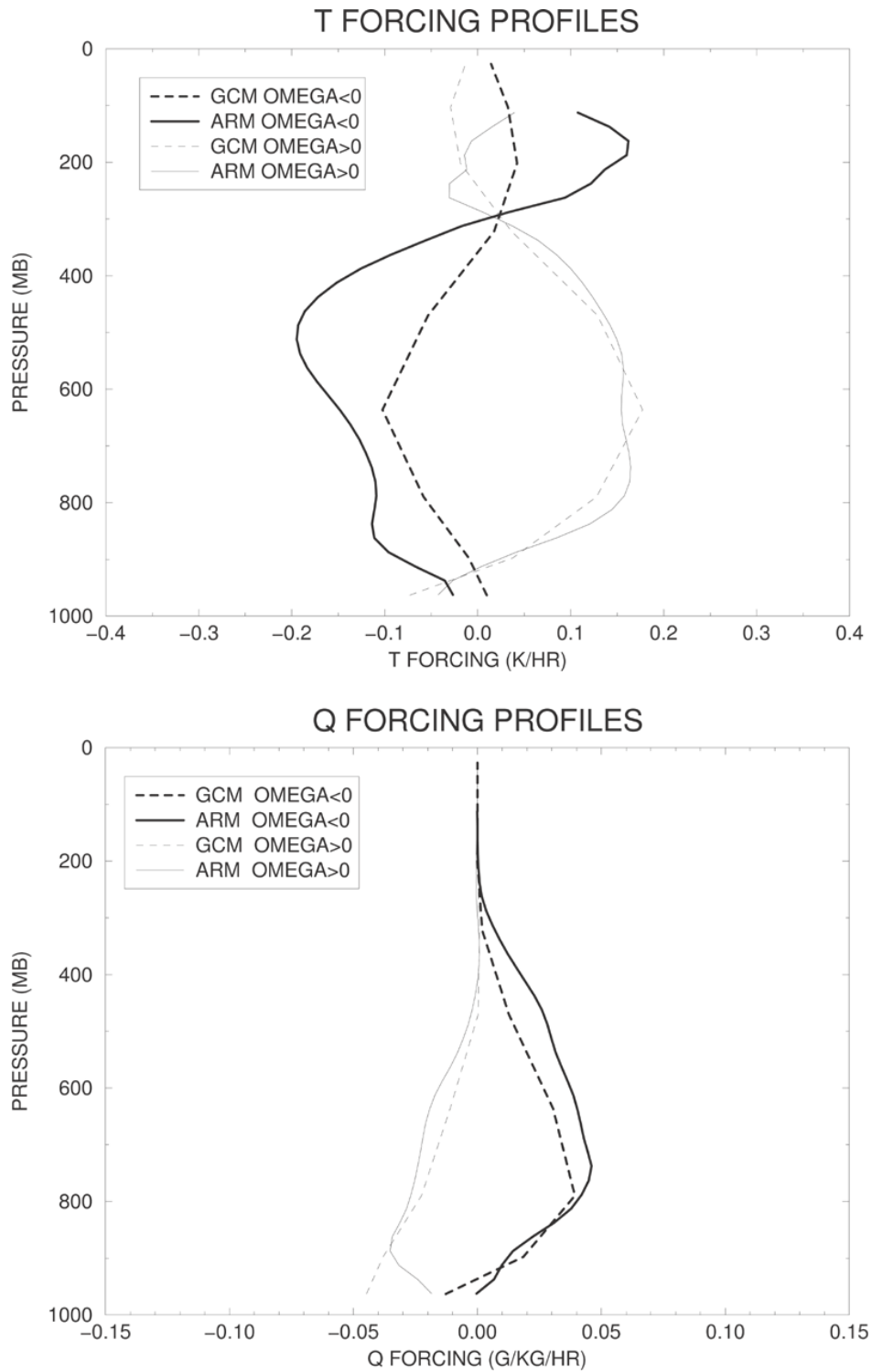
T FORCING PROFILES

Q FORCING PROFILES

Figure 1. Cold season mean advective tendencies of temperature (top) and specific humidity (bottom) for the SGP region. Solid curves: ARM continuous forcing. Dashed curves: GISS general-circulation model climatology. Bold curves: 500 mb ω < 0. Light curves: 500 mb ω > 0.
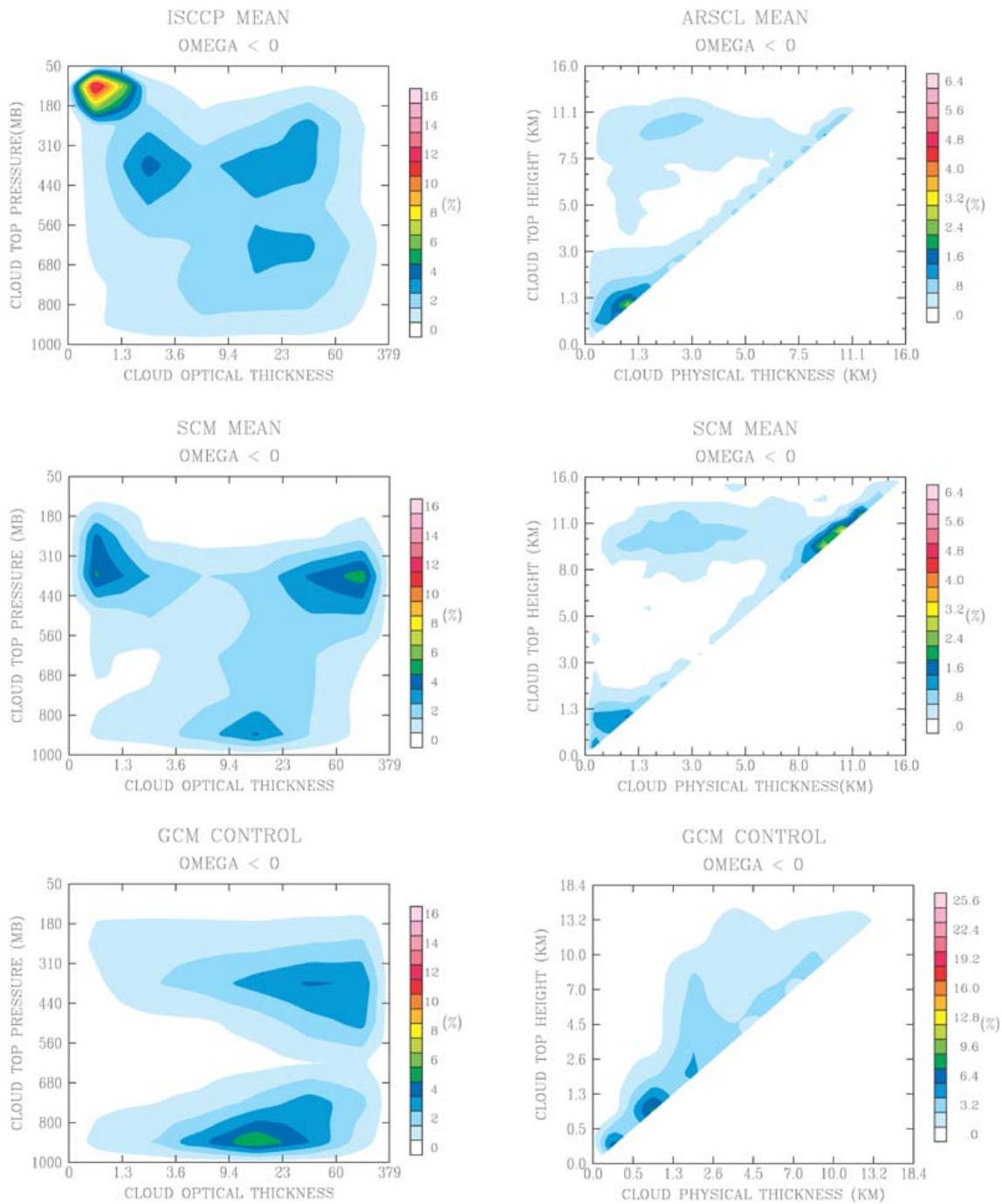
Figure 2. Cold season mean observed and simulated cloud property histograms for 500 mb $\omega < 0$. Top panels represent observations, middle panels the SCM simulation of the same time period, and bottom panels the general-circulation model climatology. The left panels are ISCCP data and simulator results portrayed as frequency of occurrence (%) as a function of cloud top pressure (mb) and column optical thickness. The right panels are ARSCL data and simulator results portrayed as frequency of occurrence as a function of height of the highest cloud top (km) and physical thickness of the layer between the highest cloud top and lowest cloud base (km). Note the different general-circulation model ARSCL simulator color scale, due to the smaller number of general-circulation model layers.

two ways—the weaker and shallower storms (Figure 1) that create a dry bias in the winter upper troposphere, and the thick (2-3 km) upper troposphere layers that prevent the production of physically thin clouds (although the GISS cloud parameterization ties to compensate by allowing for subgrid cloud thickness). The general-circulation model's low clouds are also somewhat different from observed via the presence of a second peak near 0.5 km, another effect of its discretization. Note that the general-circulation model does not overestimate high thick cloudiness in its response to its weak upper level forcing, as opposed to the SCM which does in response to the more realistic continuous forcing.

Figure 3 shows the same cloud distributions for the $\omega > 0$ regime. Not surprisingly, the major difference between this regime and the upwelling regime is the complete absence of high thick clouds and the lower frequency of occurrence of cirrus; the dominant cloud type is low physically thin but moderately optically thick stratus or stratocumulus. Many of the same ISCCP-ARSCL and SCM-general-circulation model differences described earlier are seen in this regime as well. The general-circulation model has a tendency to significantly overestimate low cloud in this regime, a behavior only slightly evident in the upwelling regime. The SCM has a small erroneous population of high physically thick clouds not detected by ARSCL (Figure 3, middle lower). However, the ISCCP simulator suggests no high optically thick clouds (Figure 3, middle upper). Thus, the apparent ARSCL simulator population is more likely due to multilayer decks of thin upper and lower level clouds rather than an actual thick single-layer cloud.

Forcing and Cloud Distribution Anomalies

Figure 4 shows the advective tendency anomaly profiles defined by the $2xCO_2 - 1xCO_2$ general-circulation model simulation differences for $\omega < 0$ and $\omega > 0$, as well as the mean of the continuous forcing anomaly profiles that are most highly correlated with the general-circulation model climate change tendency anomalies. Two versions of the continuous forcing anomaly profiles are shown, one averaged over all highly correlated timesteps (193 for $\omega < 0$, 262 for $\omega > 0$) and another for only those highly correlated timesteps for which ISCCP histograms exist (29 for $\omega < 0$, 22 for $\omega > 0$). Weather-related variability in the current climate is much stronger than climate change perturbations, so for ease of comparison the general-circulation model climate change profiles in Figure 4 have been scaled by the ratio of the vertically integrated magnitudes of the continuous forcing anomalies to those for the climate change anomalies (23.98 and 13.68 for T forcing for $\omega < 0$ and $\omega > 0$, respectively, and 27.65 and 22.30 for q forcing for $\omega < 0$ and $\omega > 0$, respectively).

General-circulation model climate change advective anomalies in upwelling situations are characterized primarily by an upward shift in the level of peak adiabatic cooling and moistening. The lower troposphere signal consists of weak warming and cooling anomalies just above and below the 800 mb level, respectively, and moderate drying below the 800 mb level. The continuous forcing contains numerous instances of forcing anomalies whose middle and upper troposphere structure closely matches that for the climate change, although the climate change anomalies tend to be somewhat larger at high levels. The best matches are less successful near the surface, consisting primarily of adiabatic warming and drying. The difference is partly compensated by the fact that the direct radiative warming due to doubling CO_2 is felt mostly near the surface.
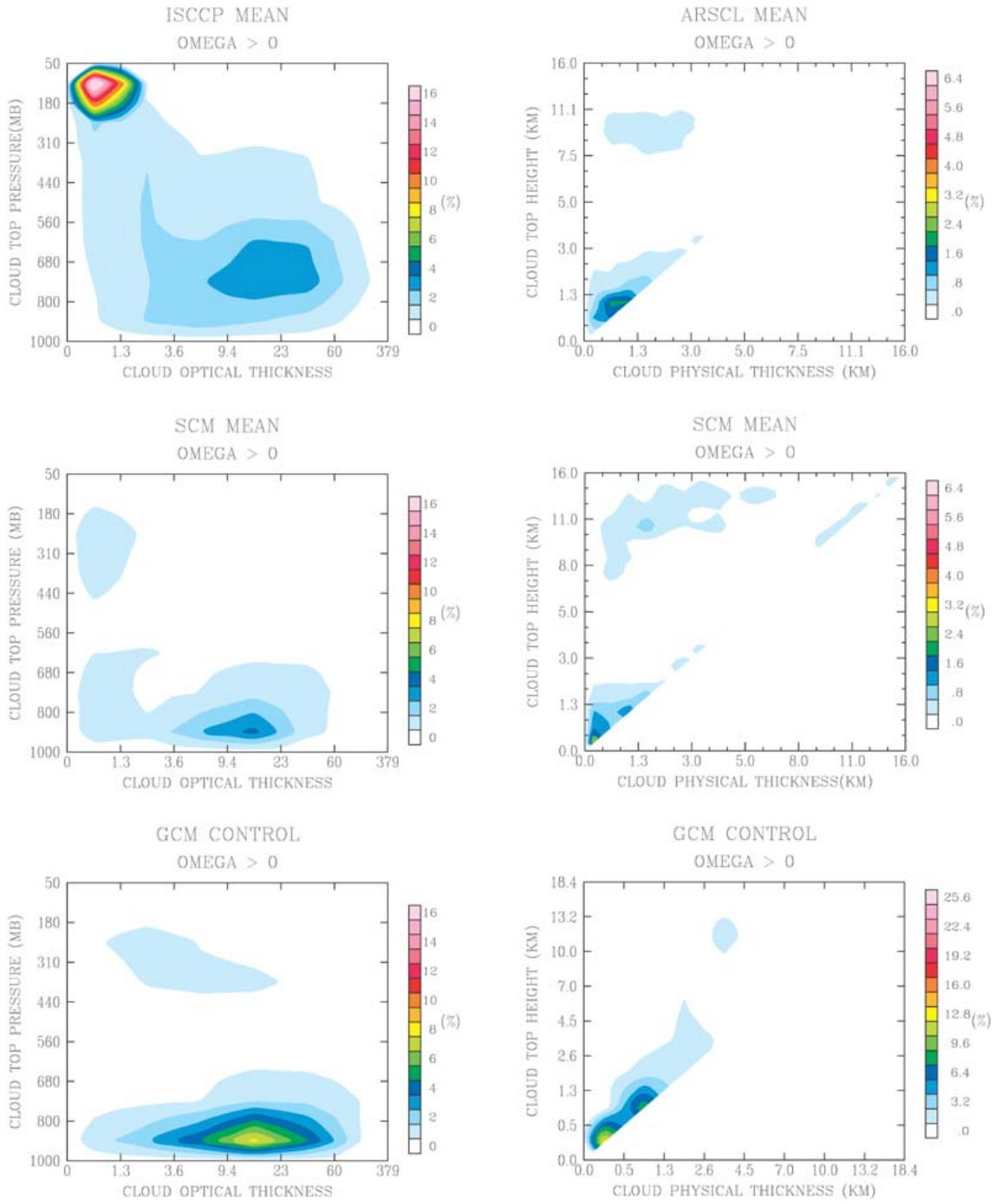
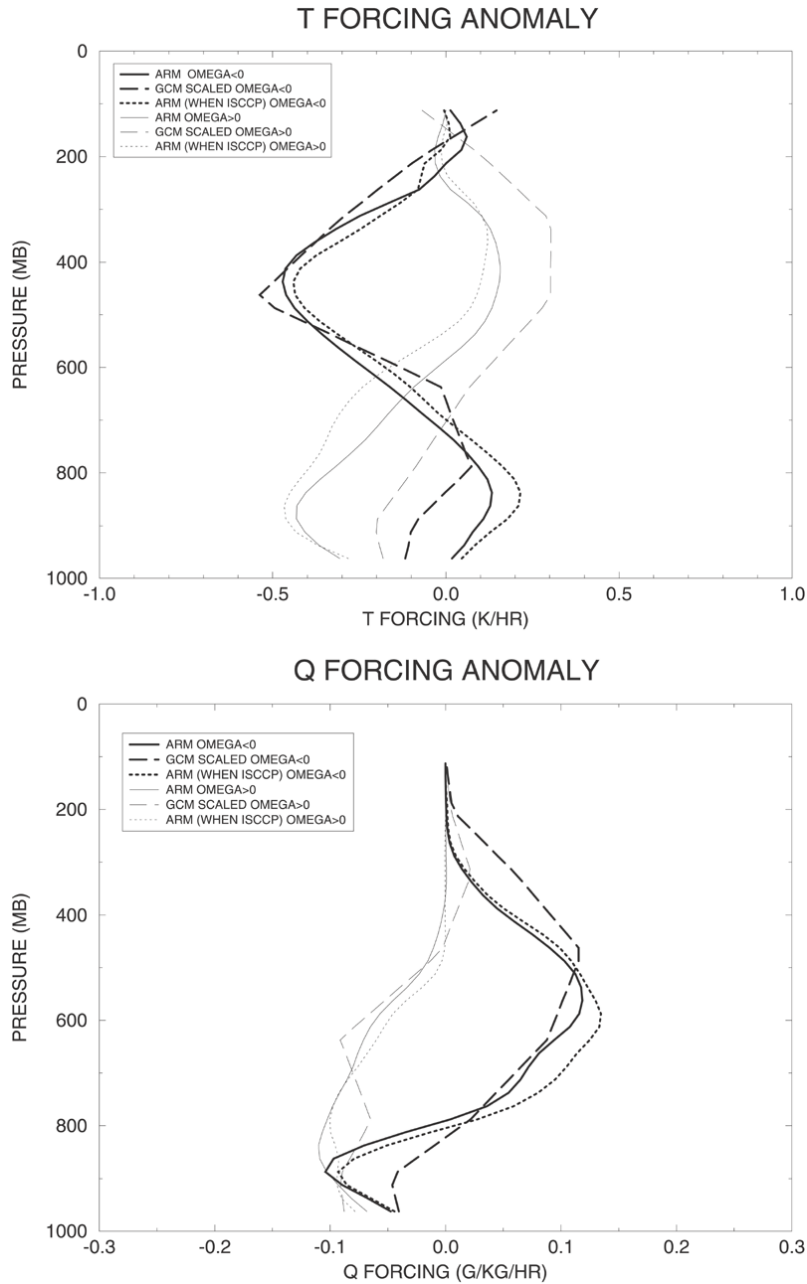**Figure 3**. As in Figure 2 but for 500 mb $\omega > 0$.

Figure 4. Anomalies of advective tendencies of temperature (top) and specific humidity (bottom) for the SGP region relative to the mean profiles in Figure 1 for times when the continuous forcing advective tendency anomalies are correlated at the 95% confidence level or greater with general-circulation model 2xCO2 – 1xCO2 advective tendency differences. Solid curves: ARM continuous forcing anomalies for all highly correlated times. Dotted curves: ARM continuous forcing anomalies for highly correlated times that have ISCCP observations. Dashed curves: General-circulation model climate change differences. Bold curves: 500 mb ω < 0. Light curves: 500 mb ω > 0. The general-circulation model curves have been scaled to have the same vertically integrated magnitude as the continuous forcing profiles for ease of comparison.

In downwelling situations, the general-circulation model climate change advective anomalies are just the opposite, defined by an upward shift in the adiabatic warming and drying peaks. The continuous forcing best matches are satisfactory for the q forcing profile but not as successful for the T forcing profile, the latter being shifted in the negative direction at all altitudes relative to the climate change profiles, i.e., weak upper level warming anomalies and stronger lower troposphere cooling anomalies.

Figure 5 shows the averaged cloud anomalies that arise in response to these dynamical forcing anomalies for the $\omega < 0$ regime. ISCCP (upper left) and ARSCL (upper right) agree on the basic pattern of cloud response: high top, thick cloud amount increases, while cirrus and all low cloud types decrease. ISCCP places the cirrus and low cloud decreases at pressures ~100 mb lower than implied by the ARSCL data. The SCM (middle left and right) reproduces the general pattern of these cloud anomalies quite well; the altitudes of peak cirrus and low cloud decrease are more consistent with ARSCL than ISCCP. The primary discrepancy between model and observation is that the SCM predicts a much larger increase in high top thick clouds, and spread over a narrower range of optical thickness, than do both of the cloud datasets.

The bottom panels of Figure 5 show the actual cloud feedback from the general-circulation model doubled CO_2 simulation in this regime. The general-circulation model's cloud feedback pattern is fairly similar to the pattern of SCM anomalies, in that both predict increases in high top thick clouds and decreases in low clouds. The general-circulation model does not predict a decrease in cirrus, but this is consistent with the lack of cirrus in its mean state associated with its coarser vertical resolution and shallower profile of advective forcing. The cloud increase is also at slightly higher altitude in the general-circulation model, an expected result given that the best match moisture advection anomaly profile in the continuous forcing dataset has weaker moistening in the upper troposphere than does the simulated climate change (Figure 4). Overall, though, the diagnostic technique appears to work as intended, and we might tentatively interpret the upper panels of Figure 5 as a glimpse of the actual cloud feedback to be expected in a warmer climate in midlatitude winter continental upwelling situations.

Figure 6 shows the corresponding cloud anomalies for the $\omega > 0$ regime. The results here are somewhat less successful in terms of dataset agreement, model performance, and consistency between current climate variability and climate change. The ISCCP and ARSCL data (upper panels) agree that low cloud cover, mostly moderate and high optical thickness but physically thin, increases, although the same cloud top location disagreement seen in earlier figures occurs here as well. More troubling is the fundamental discrepancy in cloud type decreases. ISCCP claims that all low clouds increase while cirrus fraction decreases. ARSCL sees little signal in any high cloud type but a moderate decrease in low clouds with tops at ~2 km, i.e., it gives the impression of a downward shift and physical thinning of low clouds.

The SCM (middle panels) is partly successful, given the observational uncertainty, in predicting an increase in cloudiness below ~1.5 km. However, the magnitude of this increase is less than either dataset indicates and there is no sign of a general downward shift in low cloud tops. In addition, the SCM produces a noisy pattern of small increases and decreases of cloud cover for cloud types at higher altitudes that is also inconsistent with the two datasets.
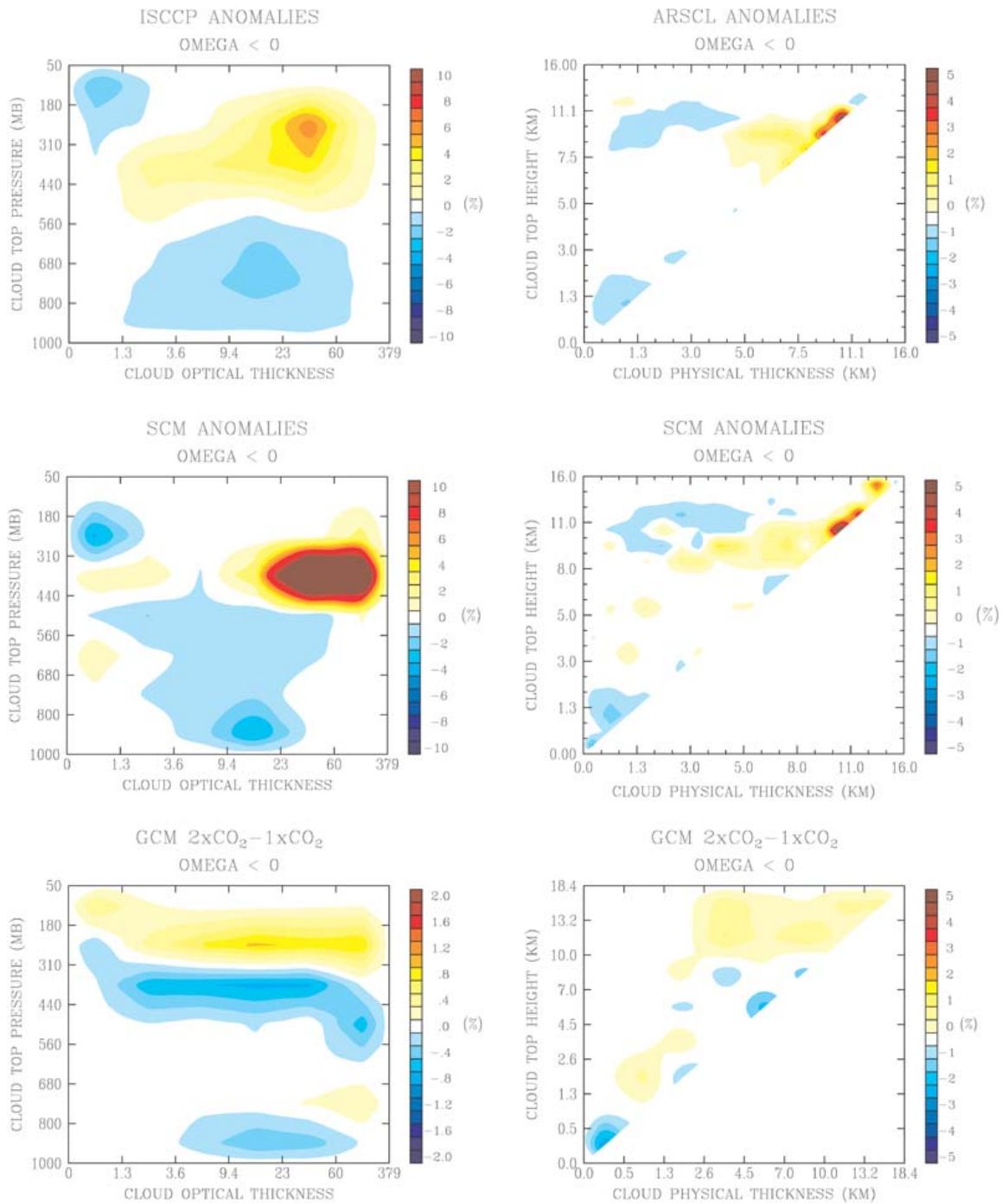
Figure 5. As in Figure 2 but for anomalies of cloud properties relative to the mean for times whose advective tendency anomalies are highly correlated with general-circulation model climate change advection differences for 500 mb $\omega < 0$. Note the different color scale for the general-circulation model ISCCP simulator anomalies due to the smaller climate change signal.
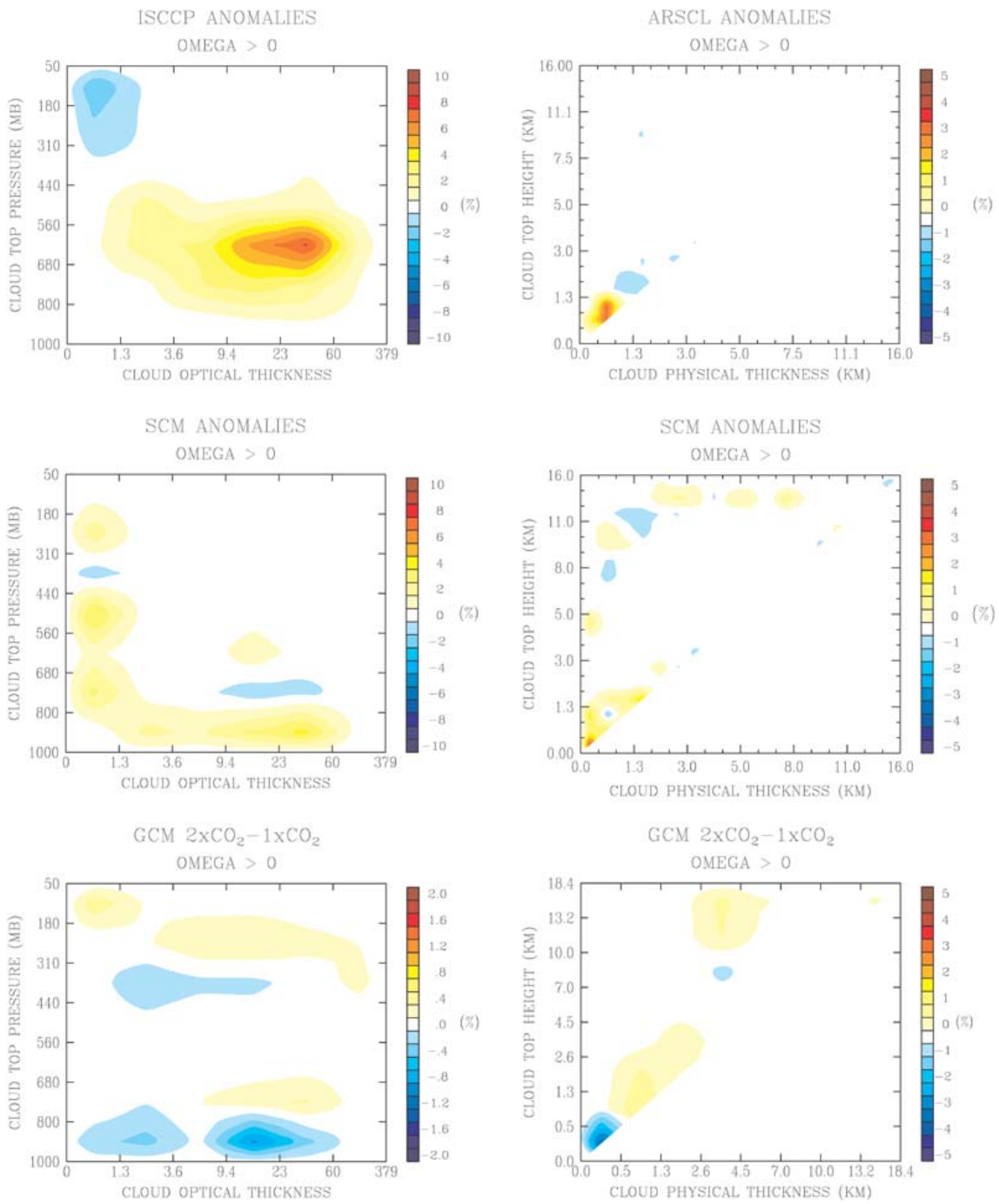
Figure 6. As in Figure 5 but for 500 mb $\omega > 0$.

The actual general-circulation model cloud feedback in the warmer climate (lower panels) looks neither like the data nor the SCM. It predicts an overall decrease and an upward shift and physical/optical thickening of low clouds with warming, and a slight upward shift in high clouds as well. The coarse layering may contribute to this different behavior as it does for the upwelling case. However, a more likely culprit is the advective forcing. It can be seen in Figure 4 that the climate change temperature forcing in particular is quite different from the best match averaged anomaly profile from the continuous forcing, even though they have similar shapes. The former has moderate upper troposphere adiabatic warming and only weak low level cooling, while the latter is dominated by strong boundary layer adiabatic cooling and only a weak upper troposphere forcing component. Thus, while the SCM-data disagreements are useful in the sense that they highlight model inadequacies that can direct parameterization research, they cannot in general provide insight about the fidelity of the general-circulation model's cloud feedback in these situations.

Discussion

ISCCP's retrieval of cloud top pressure depends on its ability to correctly partition the observed thermal infrared radiance between cloudy and clear-sky contributions. This requires knowledge of the cloud optical thickness and the atmospheric temperature and humidity profiles. For very small optical thicknesses, the retrieval does not always yield a cloud top temperature consistent with the observed tropospheric temperature profile. In such cases ISCCP places the cloud in its tropopause layer. This accounts for the large concentration of apparent thin cirrus clouds near the tropopause in the ISCCP results that has no obvious ARSCL counterpart.

For large optical thicknesses, however, most emission is from cloud top and above. Errors in cloud top pressure in such cases may occur if the atmospheric temperature and humidity profiles are incorrect. ISCCP uses the Television Infrared Observation Satellite (TIROS) Operational Vertical Sounder (TOVS) dataset for this purpose. Temperatures are provided in 15 layers from surface to stratosphere and humidity in 3 broad layers up to 300 mb, or are replaced by climatology when no TOVS retrieval is available. Pressure is inferred using the hydrostatic equation. Wang et al. (1999) show that ISCCP cloud top pressures are biased ~60 mb low due to TOVS errors for marine stratocumulus. We conducted the following tests:

1. Continuous forcing surface pressures were compared to TOVS derived surface pressures for the ISCCP cases used to produce the anomaly composite for $\omega < 0$ conditions in Figure 5. In most situations the TOVS surface pressure is in error by ~20-30 mb relative to the continuous forcing, but the errors are both positive and negative and thus are unlikely to explain a systematic low bias in cloud top pressure.

2. We chose a case (18:00 01 February 1999) in which ISCCP retrieves optically thick cloud tops primarily at 560-800 mb, while ARSCL detects cloud tops primarily between 0.3-1.5 km (the 800-1000 mb layer in ISCCP). We used the ISCCP simulator to determine the effect of TOVS temperature and humidity errors. Compared to the continuous forcing product, TOVS temperatures are ~5 K warmer in each layer; TOVS humidities are ~0.5-2 g kg^{-1} wetter from ~400-850 mb and ~2 g kg^{-1} drier below 850 mb. We placed a cloud of optical thickness $\tau = 10$ into the 800-1000 mb

layer with the TOVS profiles. The ISCCP simulator places the cloud in the 680-800 mb layer, qualitatively consistent with Wang et al.'s results but not enough to fully explain the discrepancy.

3. ISCCP retrievals can also be biased low by the presence of a thin high cloud above an optically thick lower cloud. For the case mentioned above, ARSCL detects no second cloud layer, but it too sometimes misses high, thin, low radar reflectivity clouds above thick low clouds. To test this hypothesis we placed a second cloud with varying optical thickness at 10 km altitude above the original low cloud. For $\tau = 0.5$ the retrieved cloud top remains at 680-800 mb. For $\tau = 1$ it shifts upward to the 560-680 mb layer, consistent with the actual ISCCP retrieval. For $\tau = 2$, the diagnosed cloud top pressure is 440-560 mb. Considering that the ISCCP-ARSCL disagreement is larger in the $\omega < 0$ regime, where cirrus are more plentiful, multilayer thin cirrus-contaminated scenes combined with inaccurate TOVS atmospheric state data may explain most of the ISCCP-ARSCL difference, with both datasets missing or misidentifying some thin cirrus.

We also performed a series of ISCCP simulator sensitivity tests to understand the extent to which the apparently unsatisfactory behavior of the SCM in downwelling situations (Figure 6, middle left) can be traced to differences between the actual SCM cloud field and the way it would be seen by ISCCP. First, we re-mapped the figure using the actual SCM cloud top pressures rather than the ISCCP radiatively-adjusted ones. The ISCCP technique erroneously shifts some low clouds to high altitudes; without this the SCM more clearly indicates a high cloud decrease and low cloud increase. We then built on this by adding to the lowest optical thickness category the very optically thin ($\tau < 0.1$) clouds not detected at all by ISCCP. This further strengthens the impression of high (low) cloud decrease (increase). We then added nighttime clouds, which do not contribute to the ISCCP histogram results since optical thicknesses are not available. This largely offsets the effect of the first two changes. Finally, we added hourly sampling, analogous to that used for the ARSCL simulator. This has little effect except to diminish the simulated increase in tropopause cirrus. The net effect of all the changes is something quite similar to the original ISCCP simulator result, the largest impact being on the increase in thin low clouds, some of which the ISCCP technique erroneously perceives as being thin midlevel clouds.

We also repeated the SCM ARSCL simulator calculations for both upwelling and downwelling regimes using only 1 and all 100 subgrid columns. The results are virtually indistinguishable from those presented in Figures 5 and 6 except for a slight bit of noise in the 1-column case. This robustness is not surprising given that our ARSCL simulator results are aggregated over several hundred hours.

Finally, we tested the effect of SCM overlap assumption on the ISCCP histograms. The GISS general-circulation model radiation parameterization effectively produces behavior equivalent to a mixed maximum-random overlap approach (Del Genio et al. 1996). In the upwelling regime (compare to Figure 5, middle left), a choice of random overlap spreads the region of low/midlevel cloud decrease to the lowest optical thickness categories, while maximum overlap shifts the small increase in optically thin clouds at 560-680 mb down to the 680-800 mb layer. In the downwelling regime (compare to Figure 6, middle left), random overlap slightly intensifies the increase in low optically thick clouds, while maximum overlap causes optically thin clouds at 680-800 mb to increase while those at 310-680 mb slightly decrease. None of these changes has an overall beneficial effect on the SCM.

Corresponding Author

Anthony D. Del Genio, adelgenio@giss.nasa.gov, (212)678-5588

References

Clothiaux, E. E., T. P. Ackerman, G. G. Mace, K. P. Moran, R. T. Marchand, M. Miller, and B. E. Martner, 2000: Objective determination of cloud heights and radar reflectivities using a combination of active remote sensors at the ARM CART sites. *J. Appl. Meteor.*, **39**, 645–665.

Del Genio, A. D., M.-S. Yao, W. Kovari, and K. K.-W. Lo, 1996: A prognostic cloud water parameterization for global climate models. *J. Clim.*, **9**, 270–304.

Del Genio, A. D., W. Kovari, M.-S. Yao, and J. Jonas, 2004: Cumulus microphysics and climate sensitivity. *J. Clim.,* submitted.

Klein, S. A., and C. Jakob, 1999: Validation and sensitivities of frontal clouds simulated by the ECMWF model. *Mon. Wea. Rev.*, **127**, 2514–2531.

Rossow, W. B., and R. A. Schiffer, 1999: Advances in understanding clouds from ISCCP. *Bull. Amer. Meteor. Soc.*, **80**, 2261–2288.

Wang, J., W. B. Rossow, T. Uttal, and M. Rozendaal, 1999: Variability of cloud vertical structure during ASTEX observed from a combination of rawinsonde, radar, ceilometer, and satellite. *Mon. Wea. Rev.*, **127**, 2484–2502.

Webb, M., C. A. Senior, S. Bony, and J.-J. Morcrette, 2001: Combining ERBE and ISCCP data to assess clouds in the Hadley Centre, ECMWF, and LMD atmospheric climate models. *Clim. Dyn.*, **17**, 905–922.

Xie, S.C., R.T. Cederwall, and M. Zhang, 2004: Developing long-term single-column model/cloud system-resolving model forcing data using numerical weather prediction products constrained by surface and top of the atmosphere observations. *J. Geophys. Res.*, **109**, D01104, doi:10.1029/2003JD004045.

Yao, M.-S., and A. D. Del Genio, 2002: Effects of cloud parameterization on the simulation of climate changes in the GISS GCM. Part II: Sea Surface Temperature and Cloud Feedbacks. *J. Clim.*, **15**, 2491-2503.